

## Electron-pair analysis for doubly excited ridge states

Lijun Zhang and A. R. P. Rau

*Department of Physics and Astronomy, Louisiana State University, Baton Rouge, Louisiana 70803-4001*

(Received 20 July 1992)

The two-electron Schrödinger equation is analyzed in hyperspherical coordinates, with the electrons described throughout as a pair. In contrast to the current adiabatic hyperspherical method, which reverts at large distances to a description in terms of individual electrons, the pair aspect is preserved also asymptotically. Whereas the adiabatic potential wells converge to single-ionization limits, we develop potential wells converging to the double-ionization limit of the system, and doubly excited states are then viewed as eigenstates of the pair in these wells. At the simplest level, we get series converging to the double-ionization limit which are described analytically by the "pair-Rydberg" formula, with an effective charge that increases logarithmically with the principal quantum number.

PACS number(s): 31.50.+w, 31.10.+z

### I. INTRODUCTION

Doubly excited states of atoms (or ions) display the effects of correlations between the two excited electrons. Particularly with high excitation of both electrons, their increasing liberation from the dominant central field of the positive ion enhances the importance of the correlations between them. The description of very high doubly excited states calls, therefore, for alternatives to independent-particle bases which become inadequate in the face of these strong correlations. The aim of this paper is to provide one such description.

We begin by defining the particular subset of states that is of interest to us, and the philosophy and method of our approach to calculating them, contrasting it with other theoretical approaches to doubly excited states. It is now clear from many experimental and theoretical studies that doubly excited states fall broadly into two classes [1,2], distinguished by the way the excitation energy is partitioned between the two electrons. The two electrons may either have comparable or disparate excitation. The corresponding states have been named "ridge" and "valley," respectively. This paper deals with the ridge states. Given the complete symmetry and equivalence of both electrons of the pair relative to the residual "grandparental ion" [3], the effective potential wells holding the pairs should converge to the double-ionization limit that denotes a state of the grandparent plus the pair at infinity.

These symmetrically excited ridge states have been analyzed in different ways. Rau [4], Read [3], and Wang [5] proposed phenomenologically a Rydberg formula for high excitation. Their fits to available data were extended by Molina [6]. Rost and Briggs [7] presented a diabatic molecular description for these states. Configuration-interaction and adiabatic hyperspherical methods do not separate the two classes. Of several calculations involving single-electron configurations [8], the most accurate are those of Ho [9] using complex rotation techniques, while Nicolaides and co-workers [10] using a judiciously selected symmetrical basis have somewhat more extensive

results on ridge states. The best adiabatic hyperspherical results for ridge states are those of Matsuzawa and co-workers [11], Lin and Chen [12], and Sadeghpour and Greene [13], with earlier results found by Klar and Klar [14] and Macek [15]. Other studies of ridge states are based on analytical approximations of the electron-electron interaction [16–18], and semiclassical quantization schemes [19,20].

The names ridge and valley arise from the shape of the potential in this (ion + e + e) system, which, in the case of a bare ion (that is, a point charge), takes the form (in atomic units)

$$V(\mathbf{r}_1, \mathbf{r}_2) = -Z \left[ \frac{1}{r_1} + \frac{1}{r_2} \right] + \frac{1}{r_{12}}. \quad (1)$$

This potential displays deep valleys when either  $r_1$  or  $r_2$  is close to zero, and a ridge when  $r_1 = r_2$  as discussed further below. States whose wave functions lie mainly in the valleys or around the ridge form two distinct types, distinguished in the nature of the radial correlation between the electrons. It is in the ridge states that the two electrons are on par in all aspects including specifically in their radial excitation. It is also these states that form natural partners below the double-ionization threshold to the double-escape continuum states just above that threshold, because it has long been argued that a dynamical instability arising from the mutual screening of the electrons disfavors the escape of both unless they maintain equal excitation for most of the escape [21–23]. These ideas that emphasize the viewing of both electrons together, and on par, in terms of a single entity, the "pair," underlie our approach.

As on previous occasions [21,24] when the three-body character was of the essence for the phenomena under investigation, we use collective "pair" coordinates in place of the independent-electron ones  $\mathbf{r}_1$  and  $\mathbf{r}_2$ . One set, called hyperspherical coordinates, that has proved useful, and which we adopt, defines  $(R, \alpha, \theta_{12})$  through

$$\begin{aligned}
 R &= (r_1^2 + r_2^2)^{1/2}, \\
 \alpha &= \arctan \left( \frac{r_2}{r_1} \right), \\
 \theta_{12} &= \arccos(\hat{r}_1 \cdot \hat{r}_2).
 \end{aligned} \tag{2}$$

A single radial distance  $R$  indexes the size of the system, whereas the two angles,  $\alpha$  ( $0 \leq \alpha \leq \pi/2$ ) and  $\theta_{12}$  ( $0 \leq \theta_{12} \leq 2\pi$ ), describe radial and angular correlations, respectively. In terms of them, the system's potential in (1) becomes

$$\begin{aligned}
 V(\mathbf{r}_1, \mathbf{r}_2) &\equiv \frac{C(\alpha, \theta_{12})}{R} = \frac{1}{R} \left[ -\frac{Z}{\cos\alpha} - \frac{Z}{\sin\alpha} \right. \\
 &\quad \left. + \frac{1}{(1 - \sin 2\alpha \cos \theta_{12})^{1/2}} \right].
 \end{aligned} \tag{3}$$

$R$  has become a scale variable and the essential part of  $V$  a potential surface  $C(\alpha, \theta_{12})$  which has valleys along  $\alpha=0$ ,  $\pi/2$ , and a ridge along the  $\alpha=\pi/4$  line as  $\theta_{12}$  varies (see figures in Ref. [1]). In particular, ( $\alpha=\pi/4$ ,  $\theta_{12}=0$ ) marks the peak of the potential surface (the infinite repulsion when  $\mathbf{r}_1=\mathbf{r}_2$ ) and  $\alpha=\pi/4$ ,  $\theta_{12}=\pi$  a saddle point corresponding to the configuration  $\mathbf{r}_1=-\mathbf{r}_2$ . The ridge states of interest to us are those whose wave functions are concentrated around this saddle point.

The above coordinates were used 40 years ago for the analysis of threshold double escape [21], and in the last 20 years have been used extensively for the study of doubly excited states [11–15]. These latter studies have employed a so-called adiabatic approximation, which, in analogy to the Born-Oppenheimer method, treats  $R$  as an adiabatic fixed variable while solving the angular part of the Schrödinger equation. This method has successfully described low-lying doubly excited states and given insight into the nature of correlations. However, it has also been clear that to proceed to higher excitation will require abandoning the adiabatic separation because the related continuum problem just above threshold demands handling all three variables,  $R$  and the angles, on the same footing. Also, the adiabatic method, while handling the three-body problem in the collective coordinates for small and intermediate  $R$ , departs from them at large  $R$  to return to the independent-electron coordinates for the asymptotic region. Thereby doubly excited states are viewed as successive groups that converge to individual ionization thresholds of a “parental” ion formed by (ion+ $e$ ). Having one electron remain bound, say in a principal quantum number  $N$ , while the other runs through successive values of  $n=(N, N+1, \dots, \infty)$  for the group of doubly excited states below this  $N$ th single-ionization threshold means that asymptotically the description is suited to the valleys of the potential surface:  $r_2/r_1 \rightarrow 0$ , or  $\infty$ , that is,  $\alpha \rightarrow 0$  or  $\pi/2$ , as  $R \rightarrow \infty$ .

For the very-high doubly excited ridge states that are of interest to us, we depart from the above in keeping the collective, pair description throughout, including when  $R \rightarrow \infty$ . No reference to individual electrons is made, no

single-ionization thresholds or single-electron quantum numbers invoked. The only relevant ionization limit is the one of double ionization when the “grandparental ion” (in our case, the bare nucleus) and the pair of electrons mutually separate to infinity ( $R \rightarrow \infty$ ). In the adiabatic-hyperspherical method, it has been recognized that the successive potential wells in  $R$  that converge to successive single-ionization thresholds show avoided crossings with each other. An important sequence of crossings has a locus in  $R$  which tracks the ridge line of the potential in (2). Couplings between potential curves along this locus have been recognized as providing an “excitation ladder” to high excitation [1]. A diabatic tracing of the potential along this locus would also provide a single potential well that converges finally to the double-ionization limit. Such a procedure of arriving at this well through first calculating adiabatic potential wells and then including nonadiabatic couplings between them seems, however, hopelessly cumbersome and impractical, particularly when we are interested in high-lying states. As with all Coulomb problems, the various thresholds  $N$  pile up closer and closer together and the number of adiabatic potentials and couplings grows explosively large. A more direct approach to calculating potentials that converge to the double-ionization limit is desirable and this is what we address.

Finally, before developing our method in Sec. II, we make a few remarks about other theoretical calculations of doubly excited states. Standard techniques of atomic physics such as the close-coupling method or configuration interaction have also long been used, and very successfully, for the calculation of low-lying doubly excited states. Since they involve basis functions that are products of one-electron functions, correlations mix these basis states. Strong two-electron correlations lead to large mixings and, given the diverging number of Coulomb states with increasing excitation, these calculations become impractical for the high doubly excited states. Judicious choice of basis states can extend calculations but will also fail for the high reaches of the spectrum near the double-ionization limit. Stated in terms of quantum numbers, angular correlations mix different values of  $(l_1, l_2)$ , and radial correlations of  $(N, n)$ , of the two electrons. In the limit of extreme correlation, these labels lose meaning and call for a more appropriate set of pair quantum numbers and a corresponding basis. Given the  $l$ -degeneracy of the Coulomb problem, this feature becomes important for the angular variables already for the low doubly excited states, whether of valley or ridge type. It can be analyzed by considering a fixed  $(N, n)$  manifold and the mixing of different  $(l_1, l_2)$  states contained in it [25]. Models based on the  $O(4)$  group symmetry of this restricted problem have been successful in describing this mixing and in providing alternative pair quantum numbers [26]. At low excitation, the labels  $N$  and  $n$  still retain meaning, since states of different  $(N, n)$  are separated in energy. It is now customary to label doubly excited states by these one-electron principal quantum numbers together with the  $O(4)$  quantum numbers [12]. On the other hand, at higher excitation, when different  $(N, n)$  also lie close in energy and radial correlations mix them,

all single-electron labels become deficient. This is particularly so for the high ridge states. The words “intra-shell” and “intershell” have come into vogue for describing  $(N, n)$  when  $N=n$  and  $N \neq n$ , respectively. For low doubly excited states, the former correspond to ridge and the latter to valley states. The latter have also been called “planetary” [27], in analogy with celestial mechanics where individual planets have their own distinct orbits. For the very high doubly excited states, however, the description in terms of “intra” and “inter” is no longer appropriate given the large mixing of nearly degenerate  $(N, n)$  states with both  $N$  and  $n$  large, whether equal or unequal.

## II. PAIR ANALYSIS OF TWO-ELECTRON STATES

### A. The Schrödinger equation

The two-electron Schrödinger equation in hyperspherical coordinates is well known and we record it here for completeness. For general values of the total angular momentum  $\mathbf{L}$  ( $=l_1+l_2$ ), we have [1]

$$\left[ \frac{1}{2} \left[ -\frac{d^2}{dR^2} + \frac{\Lambda^2 + \frac{15}{4}}{R^2} \right] + \frac{C(\alpha, \theta_{12})}{R} \right] [R^{5/2}\Psi(R, \Omega)] = ER^{5/2}\Psi(R, \Omega), \quad (4a)$$

where  $\Omega$  represents collectively the five angular variables,  $\alpha$ ,  $\hat{r}_1$  and  $\hat{r}_2$ . The operator  $\Lambda^2$ , called the grand angular momentum in these variables, is given by

$$\Lambda^2 = -(\sin\alpha \cos\alpha)^{-2} \frac{d}{d\alpha} \left[ \sin\alpha \cos\alpha \frac{d}{d\alpha} \right] + \frac{l_1^2}{\cos^2\alpha} + \frac{l_2^2}{\sin^2\alpha}, \quad (4b)$$

where  $l_1^2$  and  $l_2^2$  are the squared orbital-angular-momentum operators for the two electrons.

The squared grand-angular-momentum operator [1] describes collective rotations of the two electrons on the surface of a six-dimensional hypersphere. Its eigenvalues and eigenstates are

$$\Lambda^2 \Phi_{n_{RC} l_1 l_2 LM}(\Omega) = \lambda(\lambda+4) \Phi_{n_{RC} l_1 l_2 LM}, \quad (5a)$$

$$\lambda = l_1 + l_2 + 2n_{RC} = 0, 1, 2, \dots, \quad (5b)$$

$$\Phi_{n_{RC} l_1 l_2 LM}(\Omega) = c [\phi_{n_{RC} l_1 l_2 LM}(\Omega) + (-1)^{l_1+l_2-L+S+n_{RC}} \times \phi_{n_{RC} l_2 l_1 LM}(\Omega)], \quad (5c)$$

$$c = \begin{cases} \frac{1}{\sqrt{2}} & \text{if } l_1 \neq l_2 \\ \frac{1}{2} & \text{if } l_1 = l_2 \end{cases}, \quad (5d)$$

$$\begin{aligned} \phi_{n_{RC} l_1 l_2 LM} &= N_{n_{RC} l_1 l_2} (\cos\alpha)^{l_1} (\sin\alpha)^{l_2} Y_{l_1 l_2 LM}(\hat{r}_1, \hat{r}_2) \\ &\times {}_2F_1(-n_{RC}, n_{RC} + l_1 + l_2 + 2, l_2 + \frac{3}{2}; \sin^2\alpha), \end{aligned} \quad (5e)$$

$$\begin{aligned} Y_{l_1 l_2 LM}(\hat{r}_1, \hat{r}_2) &= \sum_{m_1, m_2} (l_1 l_2 LM | l_1 m_1, l_2 m_2) \\ &\times Y_{l_1 m_1}(\hat{r}_1) Y_{l_2 m_2}(\hat{r}_2). \end{aligned} \quad (5f)$$

Here  $Y$  is the familiar coupled spherical harmonic which includes a Clebsch-Gordan coefficient,  ${}_2F_1$  is a hypergeometric function, which, for the integer values of the radial correlation quantum number  $n_{RC}$  of interest, is proportional to a Jacobi polynomial [28],  $n_{RC}$  labels the nodal structure of the hyperspherical coordinate harmonics in the range  $0 < \alpha < \pi/2$ , and  $N_{n_{RC} l_1 l_2}$  is a normalization coefficient. The effective charge operator  $C(\alpha, \theta_{12})$  in (4a) is given by (3) and only depends on  $\alpha$  and  $\theta_{12}$ , while being independent of the radial size.

The different scaling in  $R$  of the angular kinetic energy and the potential in (4a) makes the two-electron equation nonseparable in hyperspherical coordinates just as it is in independent-particle coordinates. The adiabatic-hyperspherical method proceeds by seeking eigenstates of  $\Lambda^2 + RC$  at each  $R$ . Typically, a basis of products of one-electron functions is employed, and to speed convergence at large  $R$  this product is chosen so as to converge to single-ionization thresholds. Instead, we proceed as follows. Each  $\lambda$  manifold (except for  $\lambda=0$ ) is degenerate, this degeneracy increasing with  $\lambda$ . We diagonalize  $C(\alpha, \theta_{12})$  within each  $\lambda$  manifold. The eigenvectors are simultaneously eigenstates of  $\Lambda^2$  and  $C(\alpha, \theta_{12})$ . They provide at each  $R$  a basis for expansion of the full wave function  $\Psi(R, \Omega)$ , with radial functions  $F(R)$  as the expansion coefficients. The eigenvalues of  $\Lambda^2$  and  $C(\alpha, \theta_{12})$  provide diagonal potential terms (wells) in the resulting radial equations for  $F(R)$ . These potential wells converge to  $E=0$  as  $R \rightarrow \infty$ , that is, to the double-ionization limit.

In this paper we restrict ourselves to  $L=0$ . Although algebraically more involved, the extension to other  $L$  values is straightforward and we will return to it later. The  $L=0$  case has the merit of making our procedure and the form of its results more transparent. In this case, we have  $l_1=l_2=l$ , and  $\Omega$  reduces to just the two angular pair coordinates  $\alpha$  and  $\theta_{12}$ , with  $Y$  becoming

$$Y_{llM=0} = (-1)^l \left[ \frac{2l+1}{4\pi} \right]^{1/2} P_l(\cos\theta_{12}). \quad (6)$$

The functions  $\Phi$  and  $\phi$  become identical, and in  $\lambda=2(l+n_{RC})$ ,  $n_{RC}$  takes even (odd) values for  $S=0$  (1); correspondingly,  $\lambda/2$  is even (odd) for  $l+S$  even (odd). The normalized eigenfunctions of  $\Lambda^2$  for  $L=0$  are, therefore,

$$\begin{aligned} \Phi_{n_{RC} l}(\alpha, \theta_{12}) &= (-1)^l N_{n_{RC} l} \sin^l \alpha \cos^l \alpha P_l(\cos\theta_{12}) \\ &\times P_{n_{RC}}^{[l+(1/2), l+(1/2)]}(\cos 2\alpha), \end{aligned} \quad (7a)$$

TABLE I. Eigenvalues of effective charge operator  $C_{\lambda Q}$  for  $^1S$  states of He with  $\lambda \leq 20$ .

$\lambda \backslash Q$	0	1	2	3	4	5
0	-5.5902					
2	-4.6995					
4	-4.3895	-8.4413				
6	-4.2075	-6.5593				
8	-4.0823	-5.8672	-9.7461			
10	-3.9856	-5.4866	-7.5756			
12	-3.9077	-5.2413	-6.7084	-10.6039		
14	-3.8416	-5.0663	-6.2114	-8.2981		
16	-3.7848	-4.9339	-5.8832	-7.3343	-11.2443	
18	-3.7344	-4.8288	-5.6466	-6.7657	-8.8603	
20	-3.6894	-4.7427	-5.4667	-6.3825	-7.8355	-11.7555

$$N_{n_{RC}l} = 2^{2(n_{RC}+l)+1} \frac{(n_{RC}+l)!}{(2n_{RC}+2l+1)!} \times [2(2l+1)n_{RC}!(n_{RC}+2l+1)! \times (n_{RC}+l+1)]^{1/2}, \quad (7b)$$

where  $P_n^{(\alpha\beta)}$  is a Jacobi polynomial (equivalently, a Gegenbauer or ultraspherical polynomial [28]) and  $P_l$  is a Legendre polynomial.

### B. Diagonalization at fixed $\lambda$

With the eigenfunctions in (7) for a degenerate manifold  $\lambda=2(l+n_{RC})$ , we diagonalize the effective charge operator  $C(\alpha, \theta_{12})$ . The required matrix elements are

$$\langle n_{RC}l | C(\alpha, \theta_{12}) | n'_{RC}l' \rangle = \int_0^{\pi/2} \sin^2 \alpha \cos^2 \alpha d\alpha \times \int_0^\pi \sin \theta_{12} d\theta_{12} \Phi_{n_{RC}l} \Phi_{n'_{RC}l'} C(\alpha, \theta_{12}). \quad (8)$$

The matrix elements can be calculated numerically. The eigenvalues  $C_{\lambda Q}$  of this matrix are tabulated for  $^1S$  and  $^3S$  states of He [ $Z=2$  in (3)] in Tables I and II, respectively, for  $\lambda \leq 20$ , and a representative sample of  $^1S$  eigenvalues

are plotted in Fig. 1 for  $H^-$  ( $Z=1$ ). In each of these presentations, the eigenvalues divide into two groups as  $\lambda$  runs through alternate even integers and, correspondingly,  $l+S$  is alternately even and odd. The eigenvalues are labeled by  $Q=0, 1, 2, \dots$ ; the maximum value of  $Q$  is  $(\lambda-2)/4$  for odd values of  $\lambda/2$ , whereas it is  $\lambda/4$  for  $^1S$  and  $(\lambda-4)/4$  for  $^3S$  for even values of  $\lambda/2$ .

The eigenvalues have been plotted in Fig. 1 as continuous curves, although  $Q$  only takes discrete integer values, in order to show the shape of their distribution at each  $\lambda$ . In particular, these plots are strikingly similar to other diagonalizations when an external perturbation mixes states of degenerate atomic manifolds [29]. As in those examples, the extreme eigenvectors have special features, and this is shown in Figs. 2 and 3, which plot their distribution in  $(\alpha, \theta_{12})$  space. The lowest eigenvector of  $C(\alpha, \theta_{12})$ , that is, the deepest potential and therefore strongest binding, shows (Fig. 2) a concentration around  $\alpha \simeq \pi/2$  and 0 while being substantially independent of  $\theta_{12}$  for even  $\lambda/2$  [Fig. 2(a)], whereas for odd  $\lambda/2$  [Fig. 2(b)] a concentration around  $\theta_{12} \simeq 0$  and  $\pi$  and  $\alpha \simeq 0$  and  $\pi/2$ . On the other hand, the highest eigenvalue of  $C(\alpha, \theta_{12})$  exhibits [Figs. 3(a) and 3(b)] a concentration around  $\alpha \simeq \pi/4$  and  $\theta_{12} \simeq \pi$  and 0, the distribution of the eigenvector being symmetric around  $\theta_{12} \simeq \pi/2$  for even  $\lambda/2$  and antisymmetric for odd  $\lambda/2$ .

TABLE II. Eigenvalues of effective charge operator  $C_{\lambda Q}$  for  $^3S$  states of He with  $\lambda \leq 20$ .

$\lambda \backslash Q$	0	1	2	3	4
2	-7.4392				
4	-5.8854				
6	-5.3460	-9.1863			
8	-5.0529	-7.1350			
10	-4.8632	-6.3421	-10.2152		
12	-4.7264	-5.8958	-7.9703		
14	-4.6212	-5.6040	-7.0499	-10.9465	
16	-4.5364	-5.3949	-6.5138	-8.5992	
18	-4.4658	-5.2363	-6.1556	-7.6028	-11.5142
20	-4.4054	-5.1107	-5.8956	-7.00845	-9.1039

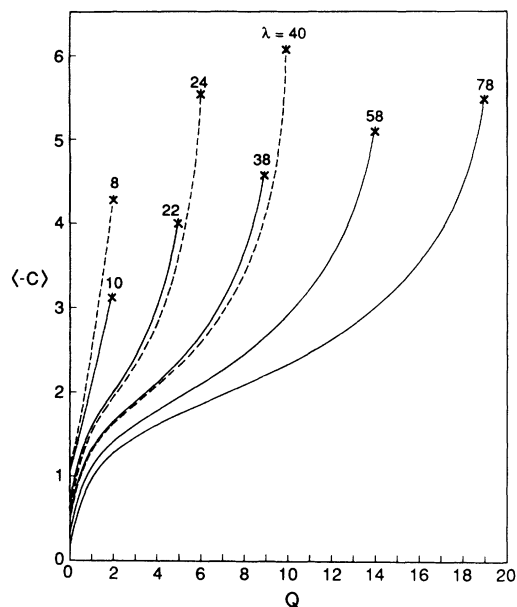


FIG. 1. Results of numerical diagonalization of (8) are shown as continuous curves, dashed (solid) for  $\lambda/2$  even (odd). Crosses give the maximum eigenvalue as given by the approximate analytical expressions in (10) and (13).

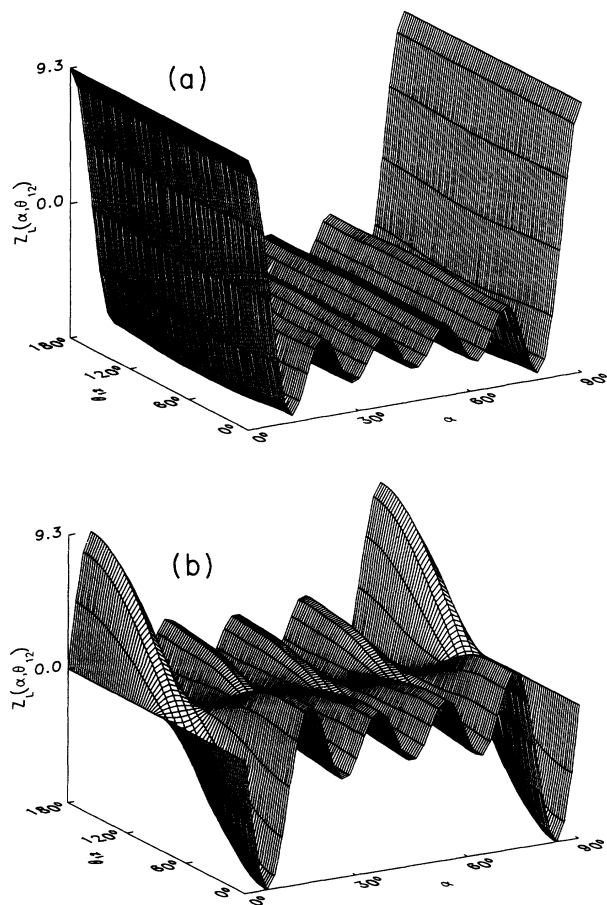


FIG. 2. The lowest eigenvector distribution in  $(\alpha, \theta_{12})$  space with  $\lambda = 20$  (a) and 18 (b).

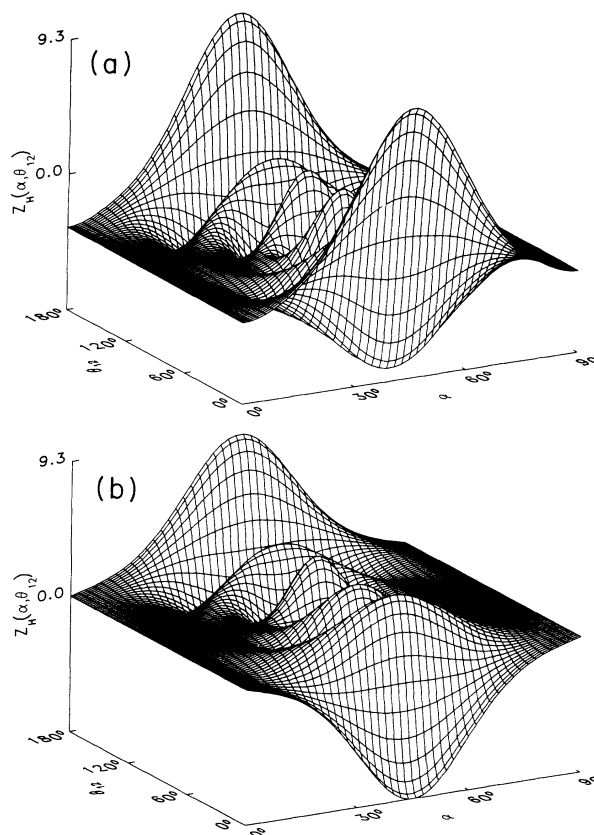


FIG. 3. The highest eigenvector distribution in  $(\alpha, \theta_{12})$  space with  $\lambda = 20$  (a) and 18 (b).

### C. Analytical results for the extreme eigenvalues

Simple but quite accurate analytical expressions for the extreme eigenvalues follow upon observing that the matrix elements of  $C$  in (8) are dominated by the diagonal terms. Table III documents this for a representative  $\lambda$ . It follows that the extreme eigenvalues are well approximated by the diagonal matrix elements in (8) with highest and lowest values of  $l$  (correspondingly, the lowest and highest values of  $n_{RC}$ ). Indeed, the symmetries noted in the previous paragraph and in Figs. 2 and 3 of the extreme eigenvectors reflect the symmetries of the function  $\Phi$  in (7) with highest and lowest allowed  $l$ . In either of these cases,  $\Phi$  in (7) takes a simple form and the matrix element can be evaluated analytically. Since it is of less interest, we do not record here the largest eigenvalue (least  $n_{RC}$ ) which corresponds to least attraction. But the most attractive potentials can be obtained as follows.

Considering  $^1S$  symmetry, when  $\lambda/2$  is even, the lowest

TABLE III. Matrix elements of  $C(\alpha, \theta_{12})$  in  $\lambda = 12$  subspace.

	$ 600\rangle$	$ 422\rangle$	$ 244\rangle$	$ 066\rangle$
$ 600\rangle$	-10.5964	-0.1575	0.7466	-0.5910
$ 422\rangle$	-0.1575	-6.6764	-0.2239	0.1488
$ 244\rangle$	0.7466	-0.2239	-5.1992	-0.2915
$ 066\rangle$	-0.5910	0.14885	-0.2915	-3.9892

eigenvalue of  $C$  is approximated by the matrix element in (8) with  $l=0$ ,  $n_{RC}=\lambda/2$ . The wave function in (7) reduces to

$$\Phi = \sqrt{8/\pi} \frac{\sin(\lambda+2)\alpha}{\sin 2\alpha}. \quad (9)$$

This gives

$$\begin{aligned} C_{\lambda, Q=\lambda/4} &\simeq \langle \frac{1}{2}\lambda, 0 | C | \frac{1}{2}\lambda, 0 \rangle \\ &= -\frac{8Z}{\pi} \sum_{k=1}^{\lambda+2} \frac{1}{2k-1} + \frac{4\sqrt{2}}{\pi} \sum_{k=1}^{\lambda+2} \frac{(-1)^{[k/2]}}{2k-1}, \end{aligned} \quad (10)$$

where  $[k/2]$  is the integer part of  $k/2$ . This value in (10), which can be thought of as an effective charge, can be simplified further, particularly for large  $\lambda$ :

$$C_{\lambda, \lambda/4} \simeq -(4/\pi) \{ Z[\gamma + \ln(4\lambda + 10)] - \sqrt{2}(0.62) \}, \quad (11)$$

where  $\gamma=0.57721$  is Euler's constant.

For an odd  $\lambda/2$ , the lowest eigenvalue of  $C$  is approximated by the matrix elements in (8) with  $l=1$ ,  $n_{RC}=(\lambda-2)/4$ . The wave function in (7) reduces to

$$\begin{aligned} \Phi = -A \frac{\cos\theta_{12}}{\sin^2 2\alpha} &[(n_{RC}+3)\sin 2(n_{RC}+1)\alpha \\ &- (n_{RC}+1)\sin 2(n_{RC}+3)\alpha], \end{aligned} \quad (12)$$

where  $A=(\sqrt{6}/8)[(n_{RC}+3)(n_{RC}+1)]^{-1/2}$ . We obtain a similar but somewhat more complicated expression than (10) involving analytical sums for

$$C_{\lambda, (\lambda-2)/4} \simeq \langle \frac{1}{2}\lambda-1, 1 | C | \frac{1}{2}\lambda-1, 1 \rangle, \quad (13)$$

which we do not display here. For large  $\lambda$ , we have analogous to (11)

$$C_{\lambda, (\lambda-2)/4} \simeq -\frac{4}{\pi} \{ Z[\gamma + \ln(4\lambda + 10)] - (Z+1) \}. \quad (14)$$

These values provided by the simple analytical expressions in (10) and (13) are marked by crosses in Fig. 1 to show that they provide an excellent approximation to the most negative eigenvalue.

#### D. An analytical pair-Rydberg formula

A first approximation to radial equations for the pair of electrons is provided by inserting the lowest eigenvalue of  $C$  for each  $\lambda$  into (4a). This provides potential wells,

$$U(R) = \frac{(\lambda + \frac{3}{2})(\lambda + \frac{5}{2})}{2R^2} + \frac{C}{R}, \quad (15)$$

with the effective charge  $C$  drawn from (10)–(14). As sketched in Fig. 4, these potential wells converge to the double-ionization limit. Each well describes a six-dimensional Coulomb problem and supports an infinity of discrete states. Singling out the lowest of these in each well provides a sequence of pair states described by the Rydberg expression

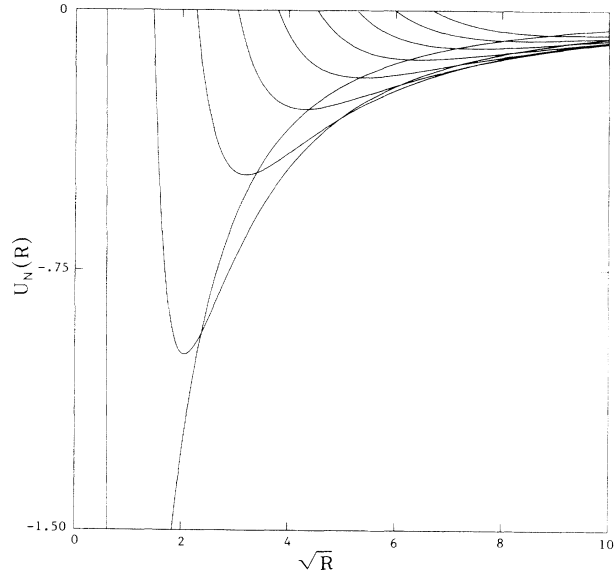


FIG. 4. Potential wells  $U(R)=[(\lambda+\frac{3}{2})(\lambda+\frac{5}{2})/2R^2] + (C_{\lambda, \lambda/4}/R)$ , with  $\lambda=0, 4, 8, 12, 16, 20, 24, 28,$  and  $32$  and  $Z=2$ .

$$E_\lambda = -\frac{C^2}{2(\lambda + \frac{5}{2})^2}, \quad (16)$$

where the  $\frac{5}{2}$  in the denominator is characteristic of the six dimensions of the pair's hyperspherical space. For  $\lambda=0, 4, 8, \dots$ , the Rydberg formula provides the approximation for what could be loosely described as the  $Ns^2$  configuration, and for  $\lambda=2, 6, 10, \dots$  for the  $Np^2$  configuration.

In Table IV we compare the results obtained from this simple analytical expression with those from other theoretical calculations for the lowest ridge states in  $H^-$  and He. The results of Ho [9] represent the best available from large numerical calculations with a basis of independent-electron functions, whereas those of Rost and Briggs [7] represent the only calculation other than ours which also has a potential well converging to the double-ionization limit (they obtain this curve through scaling from the molecular  $H_2^+$  potential). Our results are not as accurate as those obtained by these other authors for the low-lying states. Our method is really adapted to describe the very highest states and we compare with the low ones only because they are the only

TABLE IV. Eigenvalues (in a.u.) calculated by Eq. (16) for helium.

$N$	Present	Ref. [7]
1	-2.5000	-2.89065
2	-0.84135	-0.77305
3	-0.43006	-0.35290
4	-0.2670	-0.2013
5	-0.18447	-0.12995
6	-0.13633	-0.09075

available (experimental data is even more sparse). Also, in the next section we will improve on our results in Table IV by coupling multiple values of  $\lambda$ , but the specific distinction of the present results is the analytical Rydberg expression in (16). It is noteworthy that the dependence on the quantum number  $\lambda$  is not just in the Bohr-Rydberg  $\lambda^{-2}$  form but also through the dependence of the charge on  $\lambda$  as given in (11) and (14). This slow logarithmic enhancement of the binding over the standard Rydberg value can be seen as a pointer to the overlapping of manifolds that has been observed in experiment [30–33] and in theoretical calculations [13] which group states below successive parental ionization thresholds (the parental threshold energies follow a standard Rydberg trend).

### E. Coupled potential wells

Retaining only the lowest eigenvalue at each  $\lambda$  and considering each independently to give the potential in (16) is, of course, only a gross first approximation, and not expected to be accurate because of all the couplings that have been ignored. We proceed now to the next stage of off-diagonal coupling in  $\lambda$ . To take full account of this coupling we would have to consider several  $\lambda$  manifolds and all the eigenvectors in each, and evaluate matrix elements of  $C(\alpha, \theta_{12})$  between them. But, as in the adiabatic hyperspherical method, where the lowest potential wells seem to play a dominant role [11–15], we will also continue to retain only the lowest eigenvalue for each  $\lambda$ . But we will now calculate the off-diagonal matrix elements  $C_{\lambda\lambda'}$  between them. With the wave functions given in (9), these off-diagonal terms can also be evaluated analytically to give an expression analogous to (10),

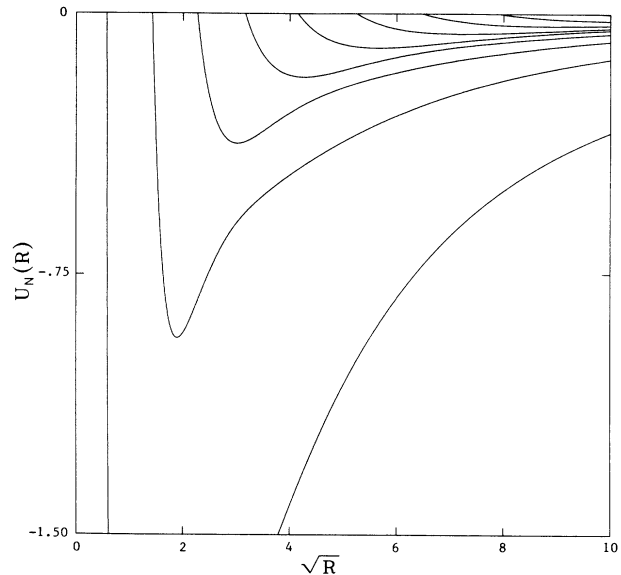


FIG. 5. Potential curves by diagonalizing the matrix given by (17) with the same  $\lambda$  values as in Fig. 4 mutually coupled together.

$$C_{\lambda\lambda'} = -\frac{8Z}{\pi} \sum_{k=(1/2)|\lambda-\lambda'|+1}^{(1/2)(\lambda+\lambda')+2} \frac{1}{2k-1} + \frac{4\sqrt{2}}{\pi} \sum_{k=(1/2)|\lambda-\lambda'|+1}^{(1/2)(\lambda+\lambda')+2} \frac{(-1)^{\lfloor \frac{k}{2} \rfloor}}{2k-1} \quad (17)$$

$$\simeq -\frac{4Z}{\pi} \ln \frac{\lambda + \lambda' + 5}{|\lambda - \lambda'| + 1}. \quad (18)$$

Similarly with the wave function given in (13), we can get the off-diagonal terms for odd  $\lambda/2$ ; these are not recorded here. Here (18) entails a further approximation for

TABLE V. Eigenvalues (in a.u.) calculated by Eq. (20), upon coupling even values of  $\lambda/2$  up to  $\lambda_{\max} = 120$ .

N	He		H <sup>-</sup>	
	Present	Ref. [7]	Present	Ref. [11]
1	-2.905 82	-2.890 65	-0.523 74	-0.525 9
2	-0.753 35	-0.773 05	-0.130 68	-0.148 79
3	-0.338 94	-0.352 90	-0.057 86	-0.069 6
4	-0.190 37	-0.201 3	-0.032 18	-0.039 925
5	-0.120 30	-0.129 95	-0.020 19	-0.026 0
6	-0.081 70	-0.090 75	-0.013 65	-0.018 205
7	-0.058 30	-0.066 95	-0.009 71	
8	-0.043 20	-0.051 4	-0.007 18	
9	-0.032 95	-0.040 73	-0.005 46	
10	-0.025 70	-0.033 06	-0.004 26	
11	-0.020 36	-0.027 37	-0.003 79	
12	-0.016 55	-0.023 03	-0.002 72	
13	-0.013 50	-0.016 95	-0.002 17	
14	-0.010 87	-0.014 78	-0.001 78	
15	-0.008 46	-0.012 8	-0.001 46	

TABLE VI. Eigenvalues (in a.u.) calculated by Eq. (20), upon coupling odd values of  $\lambda/2$  up to  $\lambda_{\max}=120$ .

N	He		H <sup>-</sup>	
	Present	Ref. [11]	Present	Ref. [11]
2	-0.644 70	-0.6053	-0.123 43	
3	-0.305 62	-0.307 185	-0.054 25	-0.0558
4	-0.175 72	-0.183 27	-0.029 61	
5	-0.113 60	-0.121 03	-0.018 81	-0.023 17
6	-0.079 20	-0.085 715	-0.012 04	-0.016 61
7	-0.050 94		-0.008 94	-0.012 505
8	-0.043 01		-0.006 52	-0.009 745
9	-0.034 17		-0.004 90	-0.0078
10	-0.025 94		-0.003 76	

large  $\lambda$  and  $\lambda'$  as before (a further small correction may be included if  $|\lambda - \lambda'|$  is not large).

Proceeding in this manner, by retaining  $\lambda$  values from 0 to some  $\lambda_{\max}$  and diagonalizing the matrix given by (10) and (17) at each  $R$ , gives potential wells  $U_N(R)$  as shown in Fig. 5 for  $\lambda_{\max}=120$ . These calculations, which require diagonalization of  $31 \times 31$  matrices, are numerically straightforward because the matrix elements themselves are calculated analytically. In Fig. 5, a mesh for  $R$  with 1600 points was chosen and the calculation took only a few min on an IBM 3090 computer. To solve for the eigenvalues of doubly excited states, the eigenvectors obtained above at each  $R$  provide a basis  $\psi_N(R; \Omega)$  for expansion of the full wave function in (4):

$$\Psi(R, \Omega) = \sum_N F_N(R) \psi_N(R; \Omega). \quad (19)$$

Inserting this into the Schrödinger equation in (4a) leads as usual, and as in the adiabatic hyperspherical scheme, to coupled equations for  $\mathbf{F}(R)$ . The coupling between different  $N$  is provided by the matrix elements  $\langle \psi_N | d/dR | \psi_{N'} \rangle$  and  $\langle \psi_N | d^2/dR^2 | \psi_{N'} \rangle$ . In this paper, we drop all these couplings off diagonal in  $N$ , in which case the eigenvalue problem reduces to that of calculating the states in each potential well in Fig. 5 independently:

TABLE VII. Eigenvalues (in a.u.) calculated by Eq. (20), with even values of  $\lambda/2$  and  $\lambda_{\max}=320$  and  $\lambda_{\max}=480$ .

N	$\lambda_{\max}=320$	$\lambda_{\max}=480$
1	-2.905 948	-2.905 948
2	-0.753 79	-0.753 81
3	-0.340 1	-0.340 16
4	-0.192 5	-0.192 69
5	-0.123 5	-0.123 74
6	-0.085 7	-0.086 04
7	-0.062 7	-0.063 18
8	-0.047 7	-0.048 27
9	-0.037 4	-0.038
10	-0.030	-0.030 63

$$\left[ \frac{1}{2} \frac{d^2}{dR^2} - U_N(R) + E \right] R^{5/2} F_N(R) = 0. \quad (20)$$

Eigenvalues obtained in this manner for H<sup>-</sup> and He are shown in Table V for even  $\lambda/2$  and Table VI for odd  $\lambda/2$ , and they represent improvements over the similar numbers in Table IV. The coupling of different  $\lambda$  converges quickly, as shown in Tables VII and VIII which contrast results for  $\lambda_{\max}=320$  and 480. As expected, the lower states reach stable values more quickly, and remain unaffected as the calculation embraces larger  $\lambda$ . A further slight shift takes place in the eigenvalues upon coupling all values of  $\lambda/2$  together, even and odd. These are displayed in Table IX, indexed by the pair principal quantum number  $N$  and the pair quantum number  $\nu$ , which describes angular correlations [2,12].

### III. DISCUSSION

This paper has presented the first steps in a well-defined program for calculating doubly excited states through analysis of the Schrödinger equation in pair (hyperspherical) coordinates. Diagonalizing the interaction at fixed values of  $\lambda$ , the grand angular momentum in the

TABLE VIII. Eigenvalues (in a.u.) calculated by Eq. (20), with odd values of  $\lambda/2$  and  $\lambda_{\max}=320$  and  $\lambda_{\max}=480$ .

N	$\lambda_{\max}=320$	$\lambda_{\max}=480$
2	-0.644 705	-0.644 705
3	-0.305 623	-0.305 624
4	-0.175 749	-0.175 753
5	-0.113 695	-0.113 703
6	-0.079 446	-0.079 463
7	-0.058 588	-0.058 622
8	-0.044 92	-0.044 984
9	-0.035 5	-0.035 613

TABLE IX. Eigenvalues (in a.u.) calculated by coupling even and odd values of  $\lambda/2$  together for He with  $\lambda_{\max} = 120$ .

$N$	$\nu$	Present
1	0	-2.926 88
2	0	-0.813 27
2	1	-0.604 47
3	0	-0.371 17
3	1	-0.279 19
4	0	-0.209 68
4	1	-0.015 87

problem, provides potential wells and angular basis functions, described throughout in pair coordinates. In particular, each of these potential wells converges at large  $R$  to the grandparental or double-ionization limit. The di-

agonalization at fixed  $\lambda$  can be carried out once and for all and even simple analytical expressions derived for the dominant eigenvalues. Extension to nondiagonal couplings in  $\lambda$  is also almost as straightforward. We have presented evidence that the resulting potential wells  $U_N(R)$  and basis functions  $\psi_N(R; \Omega)$  already give a good accounting of the organization of doubly excited states into sequences converging to the double-ionization limit, along with their energy positions. The next step of the program will be to consider the major couplings that have been left out, namely those arising from derivative terms  $d/dR$  and  $d^2/dR^2$  between the  $\psi_N$  basis states. We will return to this in a later paper but note that the numerical procedure to handle coupled equations in a single variable  $R$  is now standard. We will also extend the calculations to states of symmetry other than the  $^1S$  we have considered in this paper.

- [1] U. Fano and A. R. P. Rau, *Atomic Collisions and Spectra* (Academic, Orlando, 1986), Chap. 10.
- [2] A. R. P. Rau, in *Atomic Physics*, edited by R. S. VanDyck, Jr. and E. N. Fortson (World Scientific, Singapore, 1989), Vol. 9, p. 491.
- [3] F. H. Read, *J. Phys. B* **16**, L449 (1977); *Aust. J. Phys.* **35**, 475 (1982); *J. Phys. B* **23**, 951 (1990).
- [4] A. R. P. Rau, *J. Phys. B* **16**, L699 (1983).
- [5] H. Wang, *J. Phys. B* **19**, 3401 (1986).
- [6] Q. Molina, *Phys. Rev. A* **39**, 3298 (1989).
- [7] J. M. Rost and J. S. Briggs, *J. Phys. B* **21**, L233 (1988); **22**, 3587 (1989).
- [8] M. Aymar, *J. Phys. B* **22**, 2359 (1989).
- [9] Y. K. Ho, *Phys. Rev. A* **35**, 2035 (1987); **41**, 1492 (1990).
- [10] Y. Komninos and C. A. Nicolaides, *J. Phys. B* **19**, 1701 (1986); C. A. Nicolaides and Y. Komninos, *Phys. Rev. A* **35**, 999 (1987); M. Chrysos, Y. Komninos, Th. Mercouris, and C. A. Nicolaides, *ibid.* **42**, 2634 (1990).
- [11] H. Fukuda, N. Koyama, and M. Matsuzawa, *J. Phys. B* **20**, 2959 (1987); N. Koyama, A. Takofuji, and M. Matsuzawa, *ibid.* **22**, 553 (1989).
- [12] C. D. Lin, *Adv. Mol. Phys.* **22**, 77 (1986); Z. Chen and C. D. Lin, *Phys. Rev. A* **42**, 18 (1990).
- [13] H. R. Sadeghpour and C. H. Greene, *Phys. Rev. Lett.* **65**, 313 (1990); *Phys. Rev. A* **39**, 115 (1989); H. R. Sadeghpour, *ibid.* **43**, 5821 (1991).
- [14] H. Klar and M. Klar, *J. Phys. B* **13**, 1057 (1980).
- [15] J. H. Macek, *J. Phys. B* **1**, 831 (1968).
- [16] I. K. Dmitrieva and G. I. Plindov, *J. Phys. B* **22**, 1297 (1989).
- [17] E. de Prunele, *Phys. Rev. A* **45**, 2070 (1992).
- [18] M. Crance and L. Armstrong, Jr., *Phys. Rev. A* **26**, 694 (1982); A. R. P. Rau, *Pramana* **23**, 297 (1989); C. D. Lin and S. Watanabe, *Phys. Rev. A* **35**, 4499 (1987).
- [19] J. Muller, J. Burgdörfer, and D. Noid, *Phys. Rev. A* **45**, 1471 (1992).
- [20] G. Ezra, K. Richter, G. Tanner, and D. Wintgen, *J. Phys. B* **24**, L413 (1991).
- [21] G. H. Wannier, *Phys. Rev.* **90**, 817 (1953).
- [22] A. R. P. Rau, *Phys. Rev. A* **4**, 207 (1971); *J. Phys. (Paris) Colloq. Suppl.* **43**, C2-221 (1982).
- [23] U. Fano, *Phys. Rev. A* **22**, 2660 (1980); **24**, 2402 (1981); *Rep. Prog. Phys.* **46**, 97 (1983).
- [24] J. H. Bartlett, *Phys. Rev.* **51**, 661 (1937); V. A. Fock, *Izv. Akad. Nauk. SSR, Ser. Fiz.* **18**, 161 (1954); *K. Norsk Vidensk. Selsk. Forh.* **31**, 138 (1958).
- [25] A. R. P. Rau and Q. Molina, *J. Phys. B* **22**, 189 (1987); A. R. P. Rau, in *Aspects of Electron-Molecule Scattering and Photoionization* (New Haven, CT, 1989), edited by A. Herzenberg, AIP Conf. Proc. No. 204 (AIP New York, 1989), p. 24.
- [26] D. R. Herrick, *Adv. Chem. Phys.* **52**, 1 (1983).
- [27] I. C. Percival, *Proc. R. Soc. London Ser. A* **353**, 289 (1977).
- [28] *Handbook of Mathematical Functions*, edited by M. Abramowitz and I. A. Stegun (Dover, New York, 1965), Chaps. 15 and 22.
- [29] U. Fano, F. Robicheaux, and A. R. P. Rau, *Phys. Rev. A* **37**, 3665 (1988); A. P. R. Rau and L. Zhang, *ibid.* **42**, 6342 (1990).
- [30] S. J. Buckman and D. S. Newman, *J. Phys. B* **20**, L711 (1987).
- [31] M. Domke, C. Hue, A. Puschmann, T. Mandel, E. Hudson, D. A. Shirley, G. Kaindl, C. H. Greene, H. R. Sadeghpour, and H. Peterson, *Phys. Rev. Lett.* **66**, 1306 (1991).
- [32] P. G. Harris, H. C. Bryant, A. H. Mohagheghi, R. A. Reeder, H. Sharifian, C. Y. Tang, H. Tootoonchi, J. B. Donahue, C. R. Quick, D. C. Risløve, W. W. Smith, and J. E. Stewart, *Phys. Rev. Lett.* **65**, 309 (1990).
- [33] P. G. Harris, H. C. Bryant, A. H. Mohagheghi, R. A. Reeder, C. Y. Tang, J. B. Donahue, and C. R. Quick, *Phys. Rev. A* **42**, 6443 (1990).

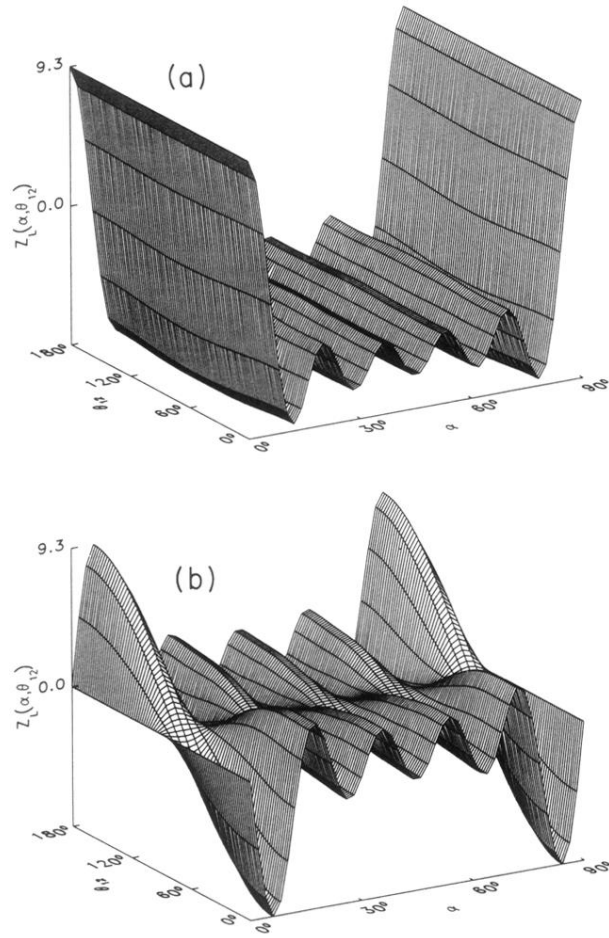


**FIG. 2.** The lowest eigenvector distribution in  $(\alpha, \theta_{12})$  space with  $\lambda = 20$  (a) and 18 (b).

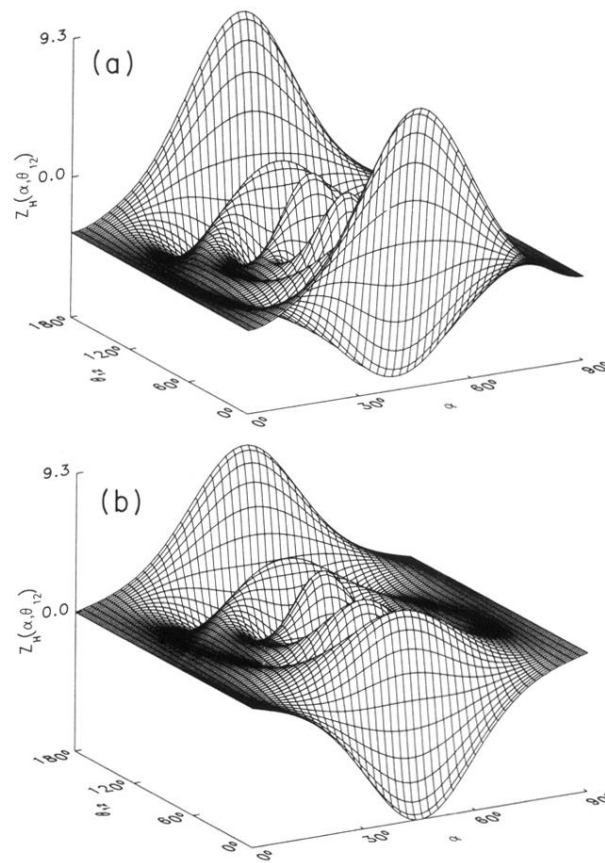


FIG. 3. The highest eigenvector distribution in  $(\alpha, \theta_{12})$  space with  $\lambda=20$  (a) and 18 (b).